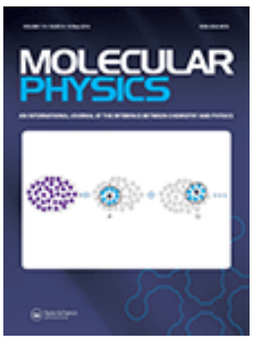

Taylor & Francis
Taylor & Francis Group

Molecular Physics

An International Journal at the Interface Between Chemistry and Physics

ISSN: 0026-8976 (Print) 1362-3028 (Online) Journal homepage: http://www.tandfonline.com/loi/tmph20

Potential application of AlN nanostructures in sodium ion batteries: a DFT study

Maziar Noei, Esmat Mohammadinasab & Nastaran Ahmadaghaei

To cite this article: Maziar Noei, Esmat Mohammadinasab & Nastaran Ahmadaghaei (2018): Potential application of AlN nanostructures in sodium ion batteries: a DFT study, Molecular Physics, DOI: 10.1080/00268976.2018.1512725

To link to this article: https://doi.org/10.1080/00268976.2018.1512725

Published online: 31 Aug 2018.

MOLECULAR PHYSICS
https://doi.org/10.1080/00268976.2018.1512725

Taylor & Francis
Taylor & Francis Group

RESEARCH ARTICLE

Potential application of AlN nanostructures in sodium ion batteries: a DFT study

Maziar Noei[a], Esmat Mohammadinasab[b] and Nastaran Ahmadaghaei[b]

[a]Department of Chemistry, Mahshahr Branch, Islamic Azad University, Mahshahr, Iran; [b]Department of Chemistry, Arak Branch, Islamic Azad University, Arak, Iran

ABSTRACT

Na-ion batteries (NIBs) appear to be a replacement for Li-ion batteries due to the nontoxicity, low cost and wide availability of sodium. Here, we explored the Na and Na^+ adsorptions on the AlN nanocluster, nanotube and nanosheet to study their potential application as an anode in NIBs, using density functional theory calculations. Based on our results, we can infer that both atomic and cationic sodium are preferentially adsorbed on a hexagon of the AlN nanostructures so that the Na^+ adsorption is very stronger than Na adsorption. By decreasing the surface curvature, the Na and Na^+ adsorptions are weakened and strengthened, respectively, and the cell voltage is increased as follows: Nanosheet ($\sim$1.48 V) > Nanotube ($\sim$1.06 V) > Nanocluster ($\sim$0.86 V). The calculated value for carbon nanotube (from literature) is about 1.45 V based on the same method. The charge separation in Al–N bonds of nanostructures has the main role in the value of cell voltage. It was predicted that by decreasing the curvature, the charge separation is increased because of decreasing the length of Al–N bonds. Based on the results, we can conclude that AlN nanosheet may be a likely applicant in NIB anode, compared to the AlN nanotube and nanocluster.

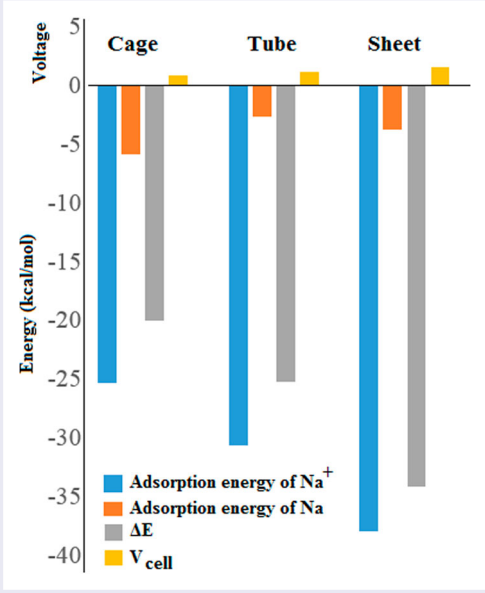

ARTICLE HISTORY
Received 24 May 2018
Accepted 25 June 2018

KEYWORDS
Nanostructures; Na-ion battery; DFT; electronic properties

1. Introduction

Li-ion batteries (LIB) are used in many portable power and electronics devices and light vehicles [1]. They display an outstanding performance in comparison to the other kinds of rechargeable batteries [2–5]. Nevertheless, there exists a worry about the low-temperature performance, cost, lifetime and safety of LIBs [6–11]. However, it seems that Na-ion batteries (NIBs) may be a replacement for LIBs due to the wide availability, low cost and nontoxicity of sodium [12,13]. Recently, synthesis of different nanostructures speeds up the development of electronic, optic and storage materials [14–24]. To date, several papers have been published on the potential application of some nanostructures in different ion

CONTACT Maziar Noei noeimaziar@gmail.com

batteries [25–30]. Previously, different types of fullerenes, nanosheets and nanotubes have been introduced as an anode electrode for ion batteries [31–34].

Carbon nanotubes display an upper Li capacity and energy storage in comparison to the graphite [33]. The performance of graphene-based LIBs is improved by substituting a few C atoms of graphene with N and B atoms [35–38]. Moreover, several inorganic nanostructures (including MgO, BN, ZnO, AlN and SiC) were explored as an anode for different ion batteries [39–43]. An important class of nanostructures are based on the AlN units such as nanotubes, nanoclusters and nanosheets, which have been widely studied as sensors, hydrogen storages, field emitters, etc. [44–53]. The AlN nanostructures have a large band gap, presenting high thermal conductivity, stability and hardness [44–55]. These features of AlN nanomaterials make them a promising candidate for use in different conditions. To date, numerous efforts have been devoted to synthesis, potential applications and characterisation of AlN nanosheets, nanocones, nanobelts, nanotubes, nanoclusters, nanowires, etc. [50–55].

The AlN nanotubes have been widely considered as chemical sensors using density functional theory (DFT) calculations. Pristine AlN nanotubes have been introduced as a chemical sensor for H_2CO gas, which cannot be detected by carbon nanotubes [56]. Anaraki has indicated that AlN nanotube is a better candidate than carbon nanotubes for application in LIBs because of producing a larger cell voltage [57]. The ammonia and nitrogen dioxide adsorption have been examined on the AlN nanosheet, demonstrating that nitrogen dioxide can be selectively detected [58]. AlN nanoclusters may be applied to sense nitric oxide gas in the presence of carbon monoxide gas [59]. Here, we investigated the potential application of three kinds of AlN nanostructures, namely nanocluster (zero dimensional, 0D), nanotube (1D) and nanosheet (2D) as an anode in NIBs by means of DFT calculations.

2. Computational methods

Density of states (DOS), frontier molecular orbital (FMO) analyses, energy calculations and optimisation of structures were performed using B3LYP/6-31G(d) method. To predict the weak interactions adequately, the dispersion term of Grimme 'D' was applied [60]. The B3LYP functional has been constantly applied to scrutinise the different behaviour of nanostructures [61–69]. We applied GAMESS program to execute all calculations [70]. The Na or Na^+ adsorption energy (E_{ad}) is computed as follows:

$$E_{ad} = E(\text{complex}) - E(\text{AlN}) - E(\text{Na/Na}^+) + E_{BSSE} \quad (1)$$

where E (AlN) is the energy of the AlN nanostructure; E (complex) is the energy of each AlN nanostructure which an Na or Na^+ is adsorbed on its surface; E_{BSSE} is the basis set superposition error energy computed by the counterpoise method [71]. The HOMO–LUMO energy gap (E_g) can be calculated using the following formula:

$$E_g = E_{LUMO} - E_{HOMO} \quad (2)$$

where E_{HOMO} and E_{LUMO} correspond to the LUMO and HOMO energies, respectively. The GaussSum program was applied to obtain the DOS plots [72]. The change of E_g as a sensitivity index of the AlN nanostructures to the Na^+ ion or Na atom is predicted as follows:

$$\Delta E_g = [(E_{g2} - E_{g1})/E_{g1}] * 100 \quad (3)$$

where E_{g1} and E_{g2} are the initial value of the E_g and the value after the Na or Na^+ adsorption, respectively.

3. Results and discussion

At the first, the adsorption of Na^+ ion, and Na atom on the AlN nanostructures will be investigated, and then their potential application as an anode in NIBs will be considered. Finally, we will compare the results.

3.1. Adsorption of Na/Na^+ on the $Al_{12}N_{12}$ nanocluster

The optimised structure of $Al_{12}N_{12}$ nanocluster is displayed in Figure 1, representing that it is constructed from 6 tetragonal, and 8 hexagonal rings with 36 Al–N bonds. The Al–N bonds are two types, including [4, 6] and [6, 6] bonds with an average length of 1.851 and 1.803 Å, respectively. The [4, 6] Al–N bonds are longer than the [6, 6] bonds because of a big strain in the tetragonal rings. The DOS plot in Figure 1 displays that the energies of HOMO and LUMO of the $Al_{12}N_{12}$ nanocluster are about −6.48 and −2.52 eV, generating an E_g value of about 3.96 eV (Table 1). At the first, we explored the adsorption of an Na^+ ion or Na atom on the wall of $Al_{12}N_{12}$ at different initial locations such as the bridge of the Al–N bonds, above the centre of the hexagons and tetragons, and above the Al and N atoms. Finally, we predicted that both of Na^+ and Na are adsorbed above the centre of tetragonal or hexagonal rings.

The calculated adsorption energies for Na^+ are about −25.3 and −22.1 kcal/mol on the hexagonal and tetragonal rings, respectively, and those of the Na atom are about −5.9 and −4.8 kcal/mol. This indicates that the favourable site for both Na and Na^+ species is the centre of the hexagonal ring, as shown in Figure 1. This phenomenon can be understood by the fact that in the case

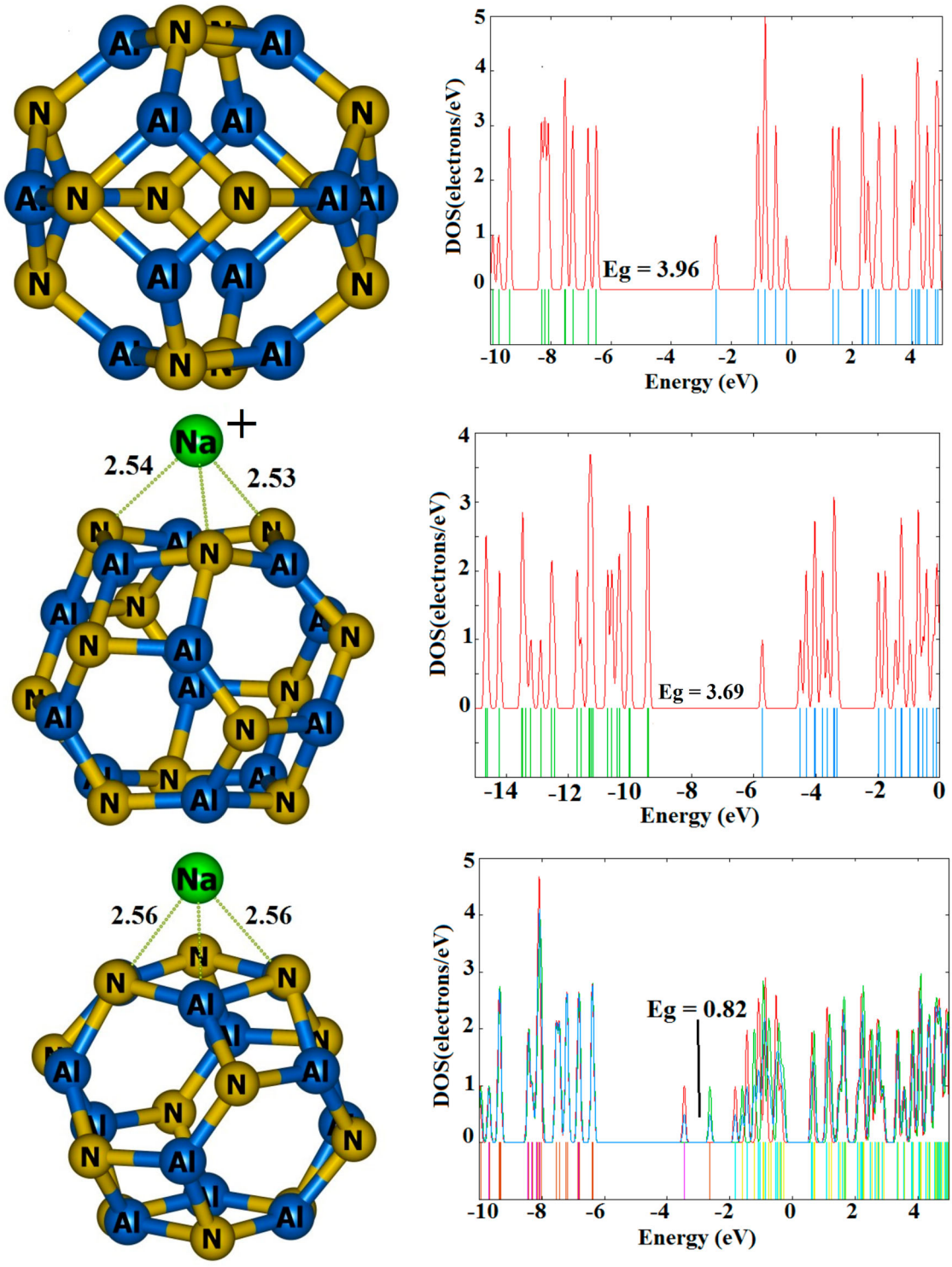

Figure 1. Optimised structures of bare AlN nanocluster and its Na^+ and Na adsorbed forms plus their DOS plots. Distances are in Å.

of adsorption on the hexagonal ring, each species interacts with three Al or N atoms but in the case of tetragonal ring, the interactions are with two atoms. In this work, we just considered the adsorption on the hexagonal ring as the most stable structures and the corresponding data are summarised in Table 1. Here, we explain why the adsorption of Na^+ is significantly stronger than that of the Na atom on the hexagonal ring of AlN nanocluster. The Na atom tends to share its valence electron with the electron deficient Al atoms of the cluster. But the N atoms adjacent to the Al sites have lone pairs, which hinder the Na atom to approach the Al sites and share its valence electron. But the Na^+ easily captures the lone pairs of N atoms of AlN nanocluster with no hindrance. Thus, the

Table 1. The adsorption energies of atomic Na and Na^+ (E_{ad}, kcal/mol) on different AlN nanostructures.

Structure	E_{ad}	E_{HOMO}	E_{LUMO}	E_g	$\%\Delta E_g$	ΔE_{cell}	V_{cell}
Cage	–	−6.48	−2.52	3.96	–	−20.0	0.86
Na^+/Cage	−25.3	−9.41	−5.72	3.69	−6.9	–	–
Na/Cage	−5.9	−3.45	−2.63	0.82	−79.3	–	–
Tube	–	−6.28	−2.18	4.11	–	−25.2	1.09
Na^+/Tube	−30.6	−8.28	−4.90	3.38	−17.8	–	–
Na/Tube	−4.4	−3.61	−2.47	1.14	−72.3	–	–
Sheet	–	−6.25	−1.51	4.74	–	−34.1	1.48
Na^+/Sheet	−37.9	−8.04	−4.68	3.36	−29.1	–	–
Na/Sheet	−3.8	−3.02	−2.07	0.95	−79.9	–	–

Notes: Energies of HOMO, LUMO and HOMO–LUMO gap (E_g) in eV. ΔE_g indicates the change of E_g of AlN nanostructures after the Na/Na^+ adsorption. The internal energy change (ΔE_{cell}, kcal/mol) and cell voltage (V_{cell}, V) of the AlN nanostructures-based Na-ion battery.

interaction of Na^+ is much stronger than that of Na atom with the AlN nanocluster.

Table 1 indicates that the adsorption of Na^+ stabilises the HOMO and LUMO levels. The HOMO is meaningfully stabilised from −6.48 to −9.41 eV, and the LUMO from −2.52 to 5.72 eV, leading to a reduction in the E_g (approximately −6.9%). The influence of adsorption of Na atom on the electronic properties of the AlN nanocluster is different from that of the adsorption of Na^+. The Na adsorption significantly makes the HOMO unstable because of an unpaired electron existing in the HOMO level of the Na/$Al_{12}N_{12}$ complex. The HOMO level shifts from −6.48 to −3.45 eV and is singly occupied. A partial DOS plot of Na/$Al_{12}N_{12}$ complex in Figure 2 demonstrates that the Na atom mainly contributes in the construction of HOMO level and in a good agreement with the severe energy change, the shape of HOMO is meaningfully changed, shifting on the Na atom. The energy of the LUMO level is slightly changed (Table 1) and Figure 2 displays that it still remains on the AlN nanocluster. As a result, the E_g is meaningfully narrowed by about 79.3%, representing that the influence of Na adsorption on the E_g of AlN nanocluster is greater than the effect of the Na^+ adsorption.

3.2. Adsorption of Na/Na^+ on the AlN nanotube

A side view of the optimised AlN nanotube is shown in Figure 3, representing that two kinds of Al–N bonds can be recognised, in which one is diagonal to the AlN tube axis and the other is parallel. All end atoms are saturated with hydrogen to reduce the boundary effects. The diameter and length of the studied AlN tube are about 5.462 and 12.371 Å, respectively. The HOMO and LUMO energies of AlN nanotube are about −6.28 and −2.18 eV, respectively. Thus, its E_g is about 4.11 eV, which is somewhat larger than that of the AlN nanocluster. In order to find the most favourable adsorption sites for Na atom or Na^+ cation on the surfaces of AlN tube, the species are located at different initial sites, including the top of N or Al atom, above the centre of the hexagon, and atop the bridge site of Al–N bonds. After careful optimisation with no constraint, both of the species preferentially are adsorbed on a hexagonal ring, as shown in Figure 3.

The adsorption energies of atomic Na and Na^+ are about −30.6 and −4.4 kcal/mol, respectively, indicating that the tube surface is much more favourable for Na^+ adsorption in comparison to the adsorption of atomic Na. Also, it was found that the adsorption of cationic Na^+ on the surface of AlN nanotube is more favourable than that on the surface of AlN nanocluster by about 5.3 kcal/mol. To understand this phenomenon, we calculated the average Mulliken charge on the N and Al

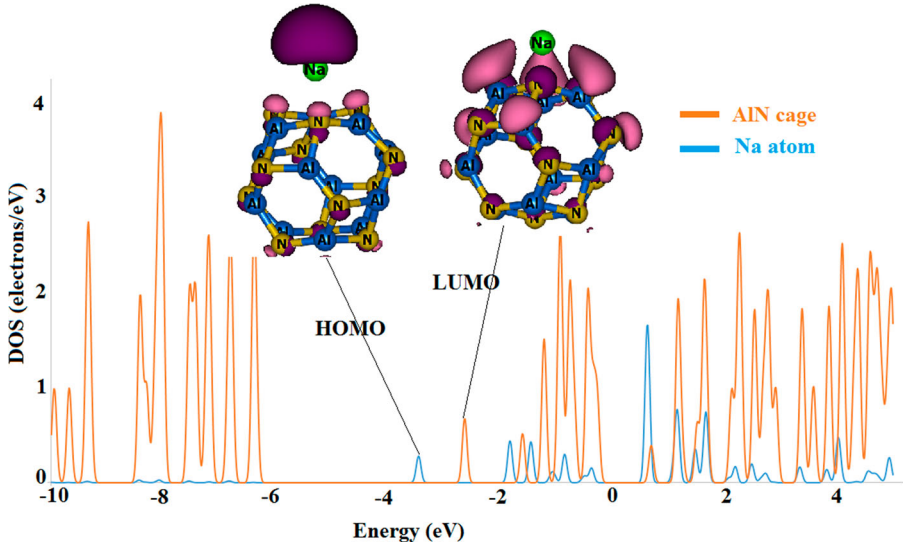

Figure 2. Partials density of states (DOS) plot of Na/AlN nanocluster. Also, the LUMO and HOMO profiles of this complex are depicted.

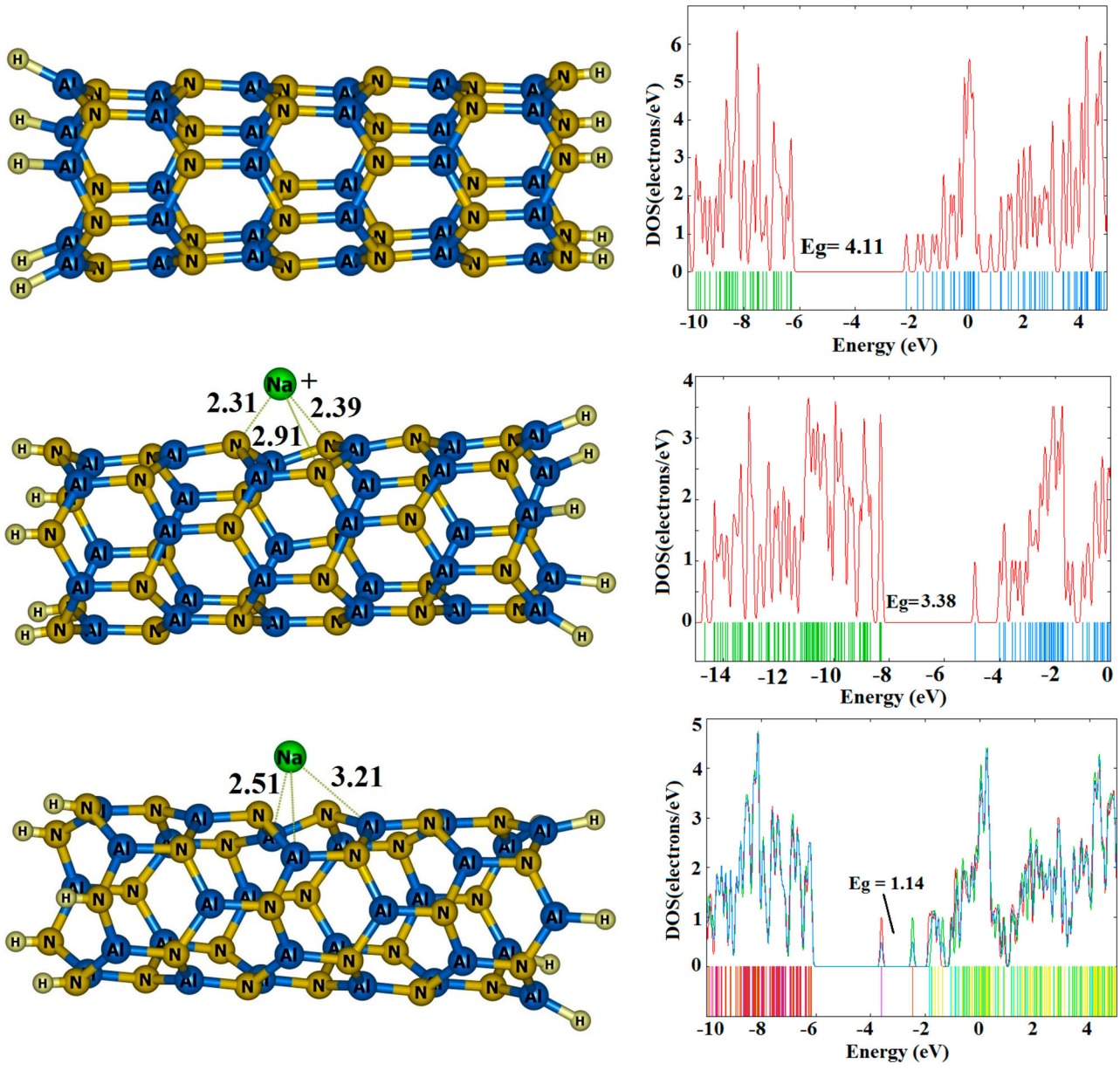

Figure 3. Optimised structures of bare AlN nanotube and its Na^+ and Na adsorbed forms plus their DOS plots. Distances are in Å.

atoms of the adsorbing hexagon of the AlN tube and nanocluster. The results show that the charge transfer from the Al atom to the N atom in the hexagon of AlN tube and nanocluster is about 0.824 and 0.743 e, respectively. This is due to the smaller average bond length of six Al–N bonds in the hexagonal rings of AlN nanotube ($\sim$ 1.816 Å) compared to that of the AlN nanocluster ($\sim$ 1.823 Å). More negative charge on the N atoms makes the adsorption of Na^+ cation more favourable and also, that of Na atom unfavourable. The results of Table 1 confirm that the adsorption of Na atom is more favourable on the AlN nanocluster compared to the AlN nanotube.

The DOS plots in Figure 3 and the summarised results in Table 1 demonstrate that similar to the case of AlN nanocluster, the electronic properties of AlN nanotube are largely affected by adsorption of Na and Na^+. In the Na/AlN tube complex, the HOMO level meaningfully destabilised by shifting from −6.48 to −3.68 eV. The LUMO level of AlN nanotube is somewhat slightly influenced by the Na adsorption. As a result, the E_g of AlN nanotube is largely reduced from 4.11 to 1.14 eV in the Na/AlN nanotube complex. This decrease in E_g will significantly increase the electrical conductivity of the AlN nanotube. These findings show that the electronic properties of the AlN nanotube are largely sensitive to the Na adsorption. Unlike the Na adsorption, after the Na^+ adsorption, both the LUMO and HOMO levels are shifted to lower energies. As a result, the E_g of AlN nanotubes is reduced after the Na^+

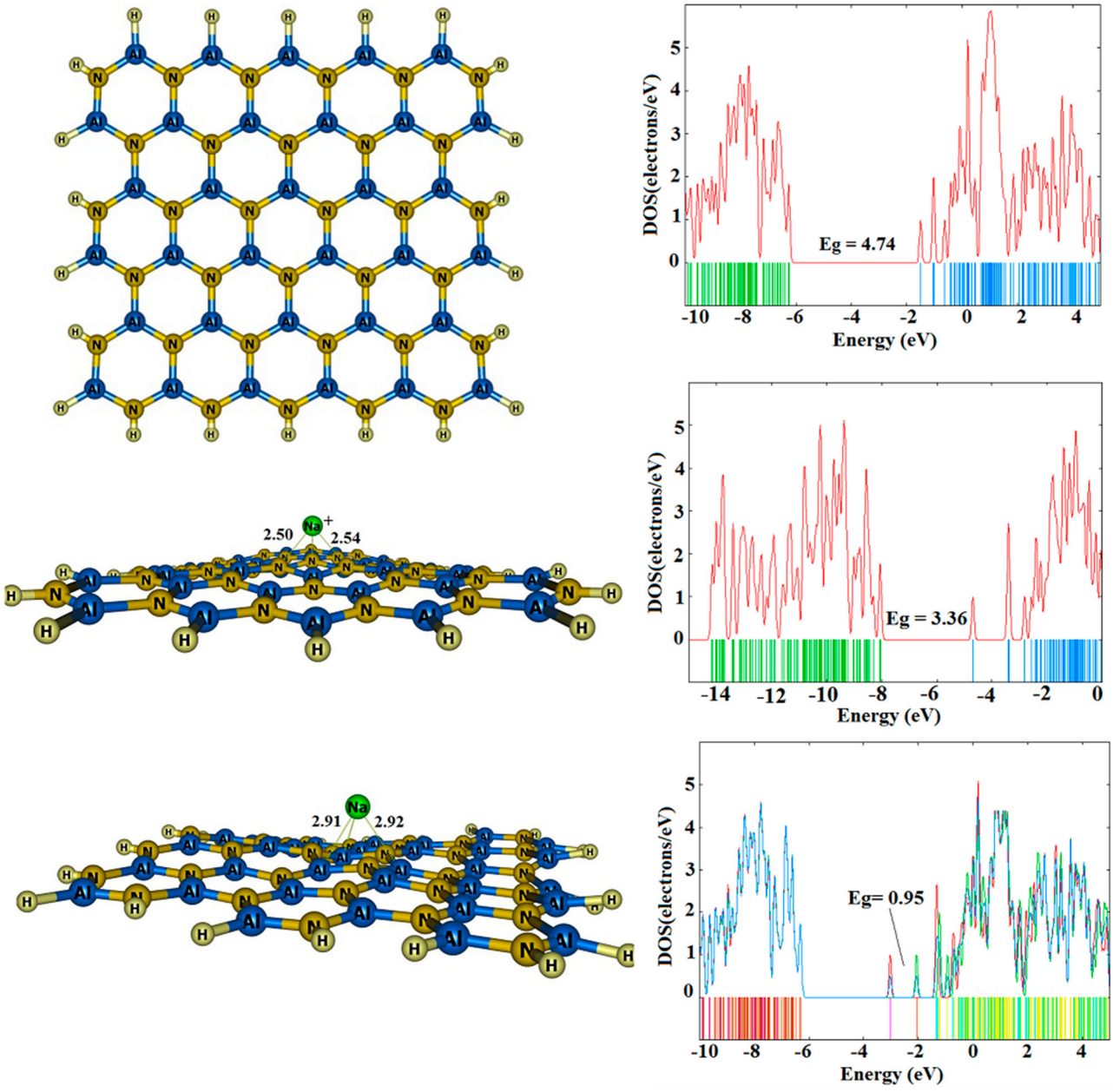

Figure 4. Optimised structures of bare AlN nanosheet and its Na^+ and Na adsorbed forms plus their DOS plots. Distances are in Å.

adsorption but its decrease is lesser than that of Na adsorption.

3.3. Adsorption of Na/Na^+ on the AlN nanosheet

We have shown the structure of AlN nanosheet in Figure 4, demonstrating that the average bond length of Al–N is about 1.805 Å, being smaller than those of AlN nanotube and nanocluster. The sheet is constructed from 33 N and 33 Al atoms, which, with its end atoms, are saturated with 22 hydrogen atoms to reduce the boundary effects. The calculated E_g for AlN nanosheet is about 4.74 eV, which is larger than that of AlN nanotube and nanocluster. Overall, by increasing the curvature of the AlN nanostructures, the E_g is decreased. Similar to the AlN nanotube, we have predicted that the Na and Na^+ are relaxed above a hexagonal ring of the AlN nanosheet, in agreement with previous results [73], as shown in Figure 4.

The adsorption energies of Na and Na^+ are predicted to be about −37.9 and −3.8 kcal/mol, respectively, representing that the adsorption of Na^+ is much more favourable than Na as discussed for AlN nanotube and nanocluster. Also, it was found that by decreasing the curvature of AlN nanostructures, the adsorption of cationic Na^+ is strengthened, and that of atomic Na is weakened.

As mentioned before, this is due to increasing the charge separation in Al–N bonds by decreasing the curvature, which is due to the reduction of the length of these bonds. The charge transfer from Al atom to the N atom in the hexagon of AlN nanosheet is about 0.851 e and the average bond length of six Al–N bonds in the hexagonal ring is about 1.805 Å. The transferred charge is larger than that in the AlN nanotube and nanocluster. The DOS plots in Figure 4 and the summarised results in Table 1 exhibit that in the Na/AlN nanosheet complex, the HOMO level shifts from −6.25 to −3.02 eV and the LUMO from −1.51 to −2.07 eV. Thus, the E_g is significantly decreased from 4.74 to 0.95 eV, which increases the electrical conductivity of the AlN nanosheet. Also, by Na^+ adsorption, both of the LUMO and HOMO levels shift to lower energies, and the E_g reduces slightly compared to the adsorption of Na.

3.4. Application of the AlN nanostructures in NIBs

If one assumes an AlN nanostructure as an anode in NIB, the reactions in the cathode and anode are simplified as follows [74–76]:

$$\text{Cathode: } Na^+ + e^- \leftrightarrow Na \tag{4}$$

$$\text{Anode: } Na/AlN \leftrightarrow Na^+/AlN + e^- \tag{5}$$

The total reaction of the cell will be as below:

$$Na^+ + Na/AlN \leftrightarrow Na^+/AlN + Na + \Delta G_{cell} \tag{6}$$

We use the Nernst equation to compute the cell voltage (V_{cell}) as follows:

$$V_{cell} = -\Delta G_{cell}/zF \tag{7}$$

where F and z are the Faraday constant (96,500 C/mol) and the charge of Na^+, respectively, and the ΔG_{cell} is Gibbs free energy change for the reaction of the cell. For DFT calculations at 0 K, we can write:

$$\Delta G_{cell} = \Delta E_{cell} + P\Delta V - T\Delta S \tag{8}$$

It has been previously revealed that the volume and entropy contributions are very small (< 0.01 V) to the cell voltage [77]. Therefore, the cell voltage for Na^+/ or Na/AlN can be predicted from Equations (6) and (8), as follows:

$$\Delta E_{cell} \sim \Delta G_{cell} = E(Na) + E\left(Na^+/AlN\right) - E\left(Na^+\right) - E(Na/\,AlN) \tag{9}$$

Based on Equation 9, the strong interaction of atomic Na with the surface of AlN nanostructures is not favourable

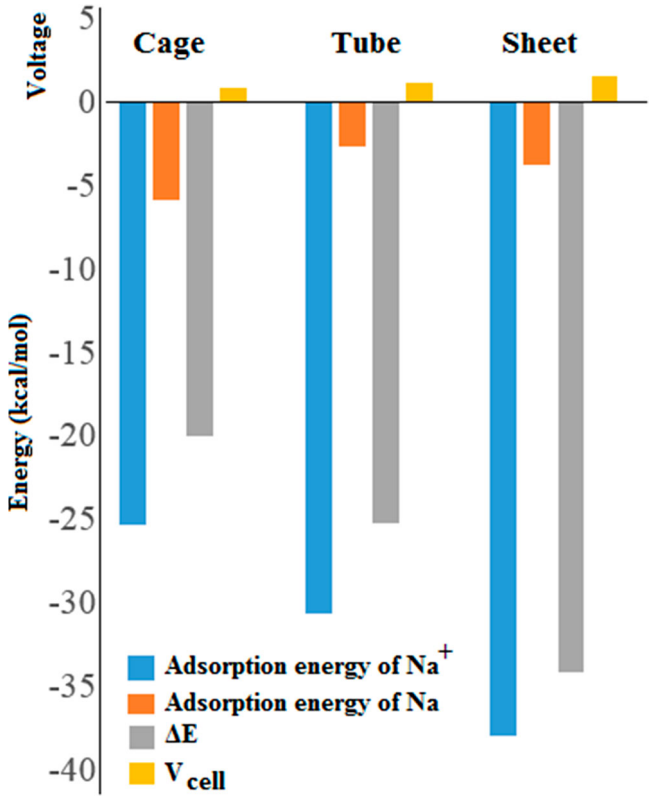

Figure 5. The plot of the cell voltage, adsorption energies for Na and Na+ in different AlN nanostructures as an anode of Na-ion batteries.

for the ΔE_{cell} and cell voltage. As shown in Table 1, the adsorption of Na^+ on all AlN nanostructures is much more favourable than that of Na, making them a promising candidate for application in the NIB anodes. The ΔE_{cell} and cell voltage were calculated for these AlN nanostructures and the results were summarised in Table 1 and plotted in Figure 5. The largest ΔE_{cell} and cell voltage are predicted to belong to the AlN nanosheet with values about −34.1 kcal/mol and 1.48 V, respectively. Gao *et al.* [75] have revealed that a carbon nanotube anode has a cell voltage of about 1.45 V for LIB based on the B3LYP/6-31G(d) method. The calculated ΔE_{cell} and cell voltage for AlN nanotube are about −25.2 kcal/mol and 1.09 V, respectively, which are significantly smaller than the corresponding values of AlN nanosheets.

Because of the stronger and weaker interactions of Na and Na^+ with AlN nanocluster, respectively, it gives less negative ΔE_{cell} and therefore, smaller cell voltage (~ 0.86 V) compared to the AlN nanosheet and nanotube. As a conclusion, our calculations suggest that the magnitude order of the cell voltage of the AlN nanostructures as an anode in NIBs is as follows: Nanosheet > nanotube > Nanocluster. This shows that by decreasing the curvature of AlN nanostructures, the

cell voltage is increased. The larger cell voltage increases the time of discharge and is very beneficial for a battery storage performance.

4. Conclusions

We examined the Na and Na^+ adsorptions on the 2D AlN nanosheet, 1D nanotube and 0D nanocluster to explore their potential application as an anode in the NIBs. It was found that the charge separation in Al–N bonds of AlN nanostructures plays the main role in generating different cell voltage. The large charge on the N atoms weakens the Na adsorption and strengthens that of Na^+, thereby increasing the cell voltage. The adsorption energy of Na^+ on the AlN nanosheet, nanotube and nanocluster is about −37.9, 30.6 and −25.3 kcal/mol and that of Na is about −3.8, −4.4 and −5.9 kcal/mol, respectively. The order of cell voltage magnitude of AlN nanostructures as an anode in NIBs is as follows: Nanosheet ($\sim$1.48 V) > Nanotube ($\sim$1.06 V) > Nanocluster ($\sim$0.86 V). This indicates that by decreasing the structural curvature, the cell voltage is increased. Our results suggest that the AlN nanosheet is more appropriate for application in the NIBs compared to the AlN nanotube and nanocluster.

Disclosure statement

No potential conflict of interest was reported by the authors.

Funding

This work was supported by Iran Nanotechnology Initiative Council.

References

[1] J.R. Dahn, T. Zheng, Y. Liu, and J. Xue, Science. **270**, 590 (1995).
[2] M.D. Johannes, K. Swider-Lyons, and C.T. Love, Solid State Ionics. **286**, 83–89 (2016).
[3] M. Armand and J.-M. Tarascon, Nature. **451**, 652–657 (2008).
[4] K. Kino, M. Yonemura, Y. Ishikawa, and T. Kamiyama, Solid State Ionics. **288**, 257–261 (2016).
[5] P.P. Prosini, C. Cento, M. Carewska, and A. Masci, Solid State Ionics. **274**, 34–39 (2015).
[6] M.D. Slater, D. Kim, E. Lee, and C.S. Johnson, Adv. Funct. Mater. **23**, 947–958 (2013).
[7] "Lithium" in *Mineral Commodity Summaries 2012* (U.S. Geological Survey, Reston, VA, 2012), p. 94.
[8] "Market," *The Lithium Site, 2012*, http://www.lithiumsite.com/ market.html (Accessed February 2012).
[9] E. Levi, Y. Gofer, and D. Aurbach, Chem. Mater. **22**, 860–868 (2009).
[10] J. Barker, M.Y. Saidi, and J.L. Swoyer, Electrochem. Solid-State Lett. **6**, A1–A4 (2003).
[11] D. Er, J. Li, M. Naguib, Y. Gogotsi, and V.B. Shenoy, ACS Appl. Mater. Interfaces. **6**, 11173–11179 (2014).
[12] V. Palomares, P. Serras, I. Villaluenga, K.B. Hueso, J. Carretero-González, and T. Rojo, Energy Environ. Sci. **5**, 5884–5901 (2012).
[13] B.J. Landi, M.J. Ganter, C.D. Cress, R.A. DiLeo, and R.P. Raffaelle, Energy Environ. Sci. **2**, 638 (2009).
[14] M. Eslami, V. Vahabi, and A.A. Peyghan, Physica E. **76**, 6–11 (2016).
[15] M. Moradi, M. Noei, and A.A. Peyghan, Mol. Phys. **111**, 3320–3326 (2013).
[16] G. Gueorguiev, J. Neidhardt, S. Stafström, and L. Hultman, Chem. Phys. Lett. **401**, 288–295 (2005).
[17] A.S. Rad, S.S. Shabestari, S.A. Jafari, M.R. Zardoost, and A. Mirabi, Mol. Phys. **114**, 1756–1762 (2016).
[18] N.L. Hadipour, A. Ahmadi Peyghan, and H. Soleymanabadi, J. Phys. Chem. C. **119**, 6398–6404 (2015).
[19] A.A. Peyghan, and H. Soleymanabadi, Mol. Phys. **112**, 2737–2745 (2014).
[20] A.A. Peyghan, S.F. Rastegar, and N.L. Hadipour, Phys. Lett. A. **378**, 2184–2190 (2014).
[21] M. Kharatha, A. Vaez, and A.S. Hasan Rozatian, Mol. Phys.. **111**, 3726–3732 (2013).
[22] A.A. Peyghan, M. Noei, and Z. Bagheri, J. Mol. Model. **20**, 2539 (2014).
[23] C. Yuan-Li, P. Xian-Feng, J. Yun, Z. Lei, Z. Juan, B. Li-Feng, L. Hai-Tao, and Y. Yong-Gang, Chin. J. Chem. **26**, 1323–1326 (2008).
[24] M. Pashangpour and A.A. Peyghan, J. Mol. Model. **21**, 116 (2015).
[25] A. Ahmadi Peyghan, H. Soleymanabadi, and Z. Bagheri, J. Mex. Chem. Soc. **59**, 67–73 (2015).
[26] K. Nejati, A. Hosseinian, L. Edjlali, and E. Vessally, J. Mol. Liq. **229**, 167–171 (2017).
[27] J. Yang, Y. Yuan, and Z. Hua, Mol. Phys. **114**, 2157–2163 (2016).
[28] S.F. Rastegar, A.A. Peyghan, and H. Soleymanabadi, Physica E. **68**, 22–27 (2015).
[29] P. Subalakshmi, and A. Sivashanmugam, J. Alloys. Compd. **690**, 523–531 (2017).
[30] B. Chen, S. Chu, R. Cai, S. Wei, R. Hu, and J. Zhou, Comput. Mater. Sci. **123**, 44–51 (2016).
[31] A.A. Peyghan and M. Noei, J. Mex. Chem. Soc. **58**, 46–51 (2014).
[32] A. Gurung, R. Naderi, B. Vaagensmith, G. Varnekar, Z. Zhou, H. Elbohy, and Q. Qiao, Electrochim. Acta. **211**, 720–725 (2016).
[33] S.W. Lee, N. Yabuuchi, B.M. Gallant, S. Chen, B.-S. Kim, P.T. Hammond, and Y. Shao-Horn, Nat. Nanotech. **5**, 531–537 (2010).
[34] M. Li, Y.-J. Liu, J.-x. Zhao, and X.-g. Wang, Appl. Surf. Sci. **345**, 337–343 (2015).
[35] L. Qie, W.M. Chen, Z.H. Wang, Q.G. Shao, X. Li, L.X. Yuan, X.L. Hu, W.X. Zhang, and Y.H. Huang, Adv. Mater. **24**, 2047–2050 (2012).
[36] Z.-S. Wu, W. Ren, L. Xu, F. Li, and H.-M. Cheng, ACS Nano. **5**, 5463–5471 (2011).
[37] Y. Liu, V.I. Artyukhov, M. Liu, A.R. Harutyunyan, and B.I. Yakobson, J. Phys. Chem. Lett. **4**, 1737–1742 (2013).
[38] R.P. Hardikar, D. Das, S.S. Han, K.-R. Lee, and A.K. Singh, Phys. Chem. Chem. Phys. **16**, 16502–16508 (2014).

[39] M. Nayebzadeh, A.A. Peyghan, and H. Soleymanabadi, Physica E. **62**, 48–54 (2014).
[40] Y. Xing, Z. Xi, Z. Xue, X. Zhang, J. Song, R. Wang, J. Xu, Y. Song, S. Zhang, and D. Yu, Appl. Phys. Lett. **83**, 1689–1691 (2003).
[41] A.A. Peyghan, S.A. Aslanzadeh, and A. Samiei, Monatshefte Chemie-Chem. Mon. **145**, 1083–1087 (2014).
[42] L.W. Yin, Y. Bando, Y.C. Zhu, M.S. Li, C.-C. Tang, and D. Golberg, Adv. Mater. **17**, 213–217 (2005).
[43] M. Menon, E. Richter, A. Mavrandonakis, G. Froudakis, and A.N. Andriotis, Phys. Rev. B. **69**, 115322 (2004).
[44] Q. Wu, Z. Hu, X. Wang, Y. Lu, X. Chen, H. Xu, and Y. Chen, J. Am. Chem. Soc. **125**, 10176–10177 (2003).
[45] J. Beheshtian, M.T. Baei, A.A. Peyghan, and Z. Bagheri, J. Mol. Model. **19**, 943–949 (2013).
[46] Q. Wu, Z. Hu, X. Wang, Y. Chen, and Y. Lu, J. Phys. Chem. B. **107**, 9726–9729 (2003).
[47] J. Beheshtian, A. Ahmadi Peyghan, and Z. Bagheri, Physica E. **44**, 1963–1968 (2012).
[48] A.A. Peyghan, M.T. Baei, S. Hashemian, and P. Torabi, J. Mol. Model. **19**, 859–870 (2013).
[49] M. Ishihara, T. Manabe, T. Kumagai, T. Nakamura, S. Fujiwara, Y. Ebata, S.-i. Shikata, H. Nakahata, A. Hachigo, and Y. Koga, Jpn. J. Appl. Phys. **40**, 5065 (2001).
[50] R. Yakimova, A. Kakanakova-Georgieva, G.R. Yazdi, G.K. Gueorguiev, and M. Syväjärvi, J. Cryst. Growth. **281**, 81–86 (2005).
[51] A. Kakanakova-Georgieva, G.K. Gueorguiev, R. Yakimova, and E. Janzén, J. Appl. Phys. **96**, 5293–5297 (2004).
[52] M.T. Baei, A.A. Peyghan, and Z. Bagheri, Superlattices Microstruct. **53**, 9–15 (2013).
[53] V. Tondare, C. Balasubramanian, S. Shende, D. Joag, V. Godbole, S. Bhoraskar, and M. Bhadbhade, Appl. Phys. Lett. **80**, 4813–4815 (2002).
[54] P. Tsipas, S. Kassavetis, D. Tsoutsou, E. Xenogiannopoulou, E. Golias, S. Giamini, C. Grazianetti, D. Chiappe, A. Molle, and M. Fanciulli, Appl. Phys. Lett. **103**, 251605 (2013).
[55] X. Zhang, Z. Liu, and S. Hark, Solid State Commun. **143**, 317–320 (2007).
[56] A. Ahmadi, N.L. Hadipour, M. Kamfiroozi, and Z. Bagheri, Sens. Actuators, B. **161**, 1025–1029 (2012).
[57] H. Anaraki-Ardakani, Phys. Lett. A. **381**, 1041–1046 (2017).
[58] S.F. Rastegar, A.A. Peyghan, H.R. Ghenaatian, and N.L. Hadipour, Appl. Surf. Sci. **274**, 217–220 (2013).
[59] J. Beheshtian, A.A. Peyghan, and Z. Bagheri, Comput. Mater. Sci. **62**, 71–74 (2012).
[60] S. Grimme, J. Comput. Chem. **25**, 1463–1473 (2004).
[61] K. Adhikari and A.K. Ray, Phys. Lett. A. **375**, 1817–1823 (2011).
[62] A.A. Peyghan, M.T. Baei, S. Hashemian, and P. Torabi, J. Cluster. Sci. **24**, 591–604 (2013).
[63] J. Du, X. Sun, and G. Jiang, Phys. Lett. A. **374**, 854–860 (2010).
[64] S. Jameh-Bozorghi and H. Soleymanabadi, Phys. Lett. A. **381**, 646–651 (2017).
[65] V. Nagarajan and R. Chandiramouli, Comput. Theor. Chem. **1049**, 20–27 (2014).
[66] X. Liu, B. Zhu, and Y. Gao, Phys. Lett. A. **380**, 1971–1975 (2016).
[67] A.A. Peyghan, M.T. Baei, and S. Hashemian, J. Cluster. Sci. **24**, 341–347 (2013).
[68] A. León and M. Pacheco, Phys. Lett. A. **375**, 4190–4197 (2011).
[69] S. Bashiri, E. Vessally, A. Bekhradnia, A. Hosseinian, and L. Edjlali, Vacuum. **136**, 156–162 (2017).
[70] M.W. Schmidt, K.K. Baldridge, J.A. Boatz, S.T. Elbert, M.S. Gordon, J.H. Jensen, S. Koseki, N. Matsunaga, K.A. Nguyen, S. Su, T.L. Windus, M. Dupuis, and J.A. Montgomery, J. Comput. Chem. **14**, 1347–1363 (1993).
[71] S.F. Boys and F. Bernardi, Mol. Phys. **19**, 553–561 (1970).
[72] N.M. O'Boyle, A.L. Tenderholt, and K. Langner, J. Comput. Chem. **29**, 839–845 (2008).
[73] A. Hosseinian, E.S. Khosroshahi, K. Nejati, E. Edjlali, and E. Vessally, J. Mol. Model. **23**, 354 (2017).
[74] D. Datta, J. Li, and V.B. Shenoy, ACS. Appl. Mater. Interfaces. **6**, 1788–1795 (2014).
[75] S. Gao, G. Shi, and H. Fang, Nanoscale. **8**, 1451–1455 (2016).
[76] Z. Bagheri, Appl. Surf. Sci. **383**, 294–299 (2016).
[77] Y.S. Meng and M.E. Arroyo-de Dompablo, Energy Environ. Sci. **2**, 589–609 (2009).